Inorg. Chem. **2004**, *43*, 4435–4446

A Series of Trinuclear $Cu^{II}Ln^{III}Cu^{II}$ Complexes Derived from 2,6-Di(acetoacetyl)pyridine: Synthesis, Structure, and Magnetism

Takuya Shiga,[†] Masaaki Ohba,*[,†,‡,§] and Hisashi Ōkawa*[,†]

Department of Chemistry, Faculty of Science, Kyushu University, Hakozaki, Higashi-ku 6-10-1, Fukuoka 812-8581, Department of Synthetic Chemistry and Biological Chemistry, Graduate School of Engineering, Kyoto University, Katsura, Nishikyo-ku, Kyoto 615-8510, and PRESTO, Japan Science and Technology Corporation (JST), Kawaguchi, Saitama 332-0012, Japan

Received August 23, 2003

A series of trinuclear $Cu^{II}Ln^{III}Cu^{II}$ complexes with the bridging ligand 2,6-di(acetoacetyl)pyridine have been prepared by one-pot reaction with $Cu(NO_3)_2 \cdot 3H_2O$ and $Ln(NO_3)_3 \cdot nH_2O$ in methanol. X-ray crystallographic studies for all the complexes indicate that two L^{2-} ligands selectively sandwich two Cu(II) ions with the 1,3-diketonate entities and one Ln(III) ion with the 2,6-acetylpyridine entity to form a trinuclear CuLnCu core bridged by the enolate oxygen atoms. Cryomagnetic properties of the complexes are studied with respect to the electronic structure of the Ln ion.

Introduction

Rational synthesis of heteronuclear metal complexes is important for elucidating specific physicochemical properties arising from interaction between neighboring metal ions.[1−6] Heteronuclear complexes comprising different 3d metal ions have been extensively studied, but 3d−4f mixed-metal complexes are less studied because of the limited number of such complexes.[7−9] One focus in the study of 3d−4f mixed-metal complexes is placed on magnetic interaction between 3d and 4f metal ions.[10−56] Gd(III) is often chosen as the 4f component because it has no orbital angular momentum and the highest spin quantum number ($S = 7/2$). Magnetic properties of 3d−Gd mixed-metal complexes can be explained by only spin−spin coupling, and a ferromagnetic interaction is confirmed between Cu(II) and Gd(III) ions.[26] Other Ln(III) ions, except for La(III) and Lu(III), have

* Author to whom correspondence should be addressed. Phone: +81-75-383-2736. Fax: +81-75-383-2732. E-mail: ohba@sbchem.kyoto-u.ac.jp.
† Kyushu University.
‡ Kyoto University.
§ Japan Science and Technology Corp.

(1) Kahn, O. *Struct. Bonding* **1987**, *68*, 89.
(2) Sinn, E.; Harris, C. M. *Coord. Chem. Rev.* **1969**, *4*, 391.
(3) Casellato, U.; Vigato, P. A. *Coord. Chem. Rev.* **1977**, *23*, 31.
(4) Zanello, P.; Tamburini, S.; Vigato, P. A.; Mazzocchin, G. A. *Coord. Chem. Rev.* **1987**, *77*, 165.
(5) Vigato, P. A.; Tamburini, S.; Fenton, D. E. *Coord. Chem. Rev.* **1990**, *106*, 25.
(6) Ōkawa, H.; Furutachi, H.; Fenton, D. E. *Coord. Chem. Rev.* **1998**, *174*, 51.
(7) Winpenny, R. E. P. *Chem. Soc. Rev.* **1998**, *27*, 447.
(8) Sakamoto, M.; Manseki, K.; Ōkawa, H. *Coord. Chem. Rev.* **2001**, *219−221*, 379.
(9) Benelli, C.; Gatteschi, D. *Chem. Rev.* **2002**, *102*, 2369.
(10) Costes, J.-P.; Dahan, F.; Dupuis, A.; Laurent, J.-P. *Inorg. Chem.* **1996**, *35*, 2400.
(11) Costes, J.-P.; Dahan, F.; Dupuis, A.; Laurent, J.-P. *Inorg. Chem.* **1997**, *36*, 3429.
(12) Costes, J.-P.; Dahan, F.; Dupuis, A.; Laurent, J.-P. *Inorg. Chem.* **1997**, *36*, 4284.
(13) Costes, J.-P.; Dupuis, A.; Laurent, J.-P. *J. Chem. Soc., Dalton Trans.* **1998**, 735.
(14) Costes, J.-P.; Dahan, F.; Dupuis, A.; Laurent, J.-P. *New J. Chem.* **1998**, 1525.
(15) Costes, J.-P.; Dahan, F.; Dupuis, A.; Laurent, J.-P. *Chem.−Eur. J.* **1998**, *4*, 1616.
(16) Costes, J.-P.; Dupuis, A.; Laurent, J.-P. *Eur. J. Inorg. Chem.* **1998**, *10*, 1543.
(17) Costes, J.-P.; Dahan, F.; Dupuis, A. *Inorg. Chem.* **2000**, *39*, 165.
(18) Costes, J.-P.; Dahan, F.; Dupuis, A.; Laurent, J.-P. *Inorg. Chem.* **2000**, *39*, 169.
(19) Costes, J.-P.; Dahan, F.; Dupuis, A. *Inorg. Chem.* **2000**, *39*, 5994.
(20) Costes, J.-P.; Dahan, F.; Donnadieu, B.; García-Tojal, J.; Laurent, J.-P. *Eur. J. Inorg. Chem.* **2001**, *2*, 363.
(21) Costes, J.-P.; Dahan, F.; García-Tojal, J. *Chem.−Eur. J.* **2002**, *8*, 5430.
(22) Bencini, A.; Benelli, C.; Caneschi, A.; Carlin, R. L.; Dei, A.; Gatteschi, D. *J. Am. Chem. Soc.* **1985**, *107*, 8128.
(23) Bencini, A.; Benelli, C.; Caneschi, A.; Dei, A.; Gatteschi, D. *Inorg. Chem.* **1986**, *25*, 572.
(24) Benelli, C.; Caneschi, A.; Gatteschi, D.; Guillou, O.; Pardi, L. *Inorg. Chem.* **1990**, *29*, 1750.
(25) Andruh, M.; Bakalbassis, E.; Kahn, O.; Trombe, J. C.; Porcher, P. *Inorg. Chem.* **1993**, *32*, 1616.
(26) Andruh, M.; Ramade, I.; Codjovi, E.; Guillou, O.; Kahn, O.; Trombe, J. C. *J. Am. Chem. Soc.* **1993**, *115*, 1822.
(27) Ramade, I.; Kahn, O.; Jeannin, Y.; Robert, F. *Inorg. Chem.* **1997**, *36*, 930.
(28) Avecilla, F.; Platas-Iglesias, C.; Rodríguez-Cortiñas, R.; Guillemot, G.; Bünzli, J.-C. G.; Brondino, C. D.; Geraldes, C. F. G. C.; Blas, A. d.; Rodríguez-Blas, T. *Dalton Trans.* **2002**, 4658.

10.1021/ic034998l CCC: $27.50
Published on Web 06/11/2004

an orbital angular momentum, and analyses of the magnetic properties of mixed-metal complexes with these Ln(III) ions are complicated by a contribution from the orbital angular momentum. To evaluate magnetic interaction between 3d and 4f metal ions, an empirical approach based on comparison with analogous compounds with a diamagnetic 3d ion is adopted.[15,50,55] Costes et al.[15] used $Ni^{II}Ln^{III}$ ($S_{Ni} = 0$) complexes as references for analyzing the magnetic interaction of $Cu^{II}Ln^{III}$ complexes; $\Delta\chi$ ($= \chi_{CuLn} - \chi_{NiLn}$) is considered as a measure of magnetic interaction between Cu(II) and Ln(III) ions. Similarly, Kahn et al.[50] used Ln_2Zn_3 complexes as the references for analyzing the magnetic interaction of Ln_2Cu_3 complexes. In this study, however, the mixed-metal complexes of limited Ln(III) ions are treated and the effect of the electronic configuration of the Ln ion upon magnetic interaction is not fully elucidated. Apart from 3d−4f mixed-metal complexes, radical−Ln(III) complexes have been prepared and studied in magnetic properties.[57−60]

In the present work 2,6-di(acetoacetyl)pyridine (H_2L) is employed as the bridging ligand for preparing 3d−4f heteronuclear complexes due to its potential selection of different metals. The ligand (L^{2-}) has three metal-binding sites, one central 2,6-diacetylpyridine site and two terminal 1,3-diketonate sites, sharing enolate oxygen atoms. Mixed-metal $Cu^{II}Ln^{III}Cu^{II}$ complexes with a general formula of $Cu_2Ln(L)_2(NO_3)_3$ have been derived from H_2L for the series of Ln^{III} ions (except for Pm) and Y^{III} ion by one-pot reaction with $Cu(NO_3)_2{\cdot}3H_2O$ and $Ln(NO_3)_3{\cdot}nH_2O$ in methanol. X-ray crystallographic studies have proved that two L^{2-} ligands accommodate two Cu(II) ions with the 1,3-diketone site and one Ln(III) ion with the 2,6-diacylpyridine site, affording trinuclear $Cu^{II}Ln^{III}Cu^{II}$ complexes. Magnetic properties of the complexes are reported.

Experimental Section

Materials. 2,6-Di(acetoacetyl)pyridine (H_2L) was prepared according to the literature method.[61] Other chemicals were of reagent grade and used as purchased.

Synthesis of the $Cu_2Ln(L)_2$ Complexes (Ln = Lanthanide Ion). A series of CuLnCu complexes were obtained by one-pot reaction of H_2L, $Cu(NO_3)_2{\cdot}3H_2O$, and $Ln(NO_3)_3{\cdot}nH_2O$ (2:2:1) in methanol. Two synthetic procedures were adopted. A complete list of compounds prepared with their numbering and analytical data is given in Table 1.

Procedure 1 (1−12, 15). To a solution of $Cu(NO_3)_2{\cdot}3H_2O$ (1.0 mmol) and $Ln(NO_3)_3{\cdot}nH_2O$ (0.5 mmol) in hot methanol (ca. 50 cm^3) was added a hot methanolic solution (ca. 50 cm^3) of H_2L (1.0 mmol). The reaction mixture was stirred for a few minutes and allowed to stand to obtain green crystals of $[Cu_2La(L)_2(NO_3)_3(MeOH)_2]$ (**1′**), $[Cu_2Ln(L)_2(NO_3)_2(MeOH)_2]NO_3{\cdot}n$(MeOH) (Ln = Ce, $n = 3$ (**2′**); Ln = Pr, $n = 3$ (**3′**); Ln = Nd, $n = 3$ (**4′**); Ln = Sm, $n = 0$ (**5′**); Ln = Gd, $n = 0$ (**7′**); Ln = Dy, $n = 1$ (**9′**); Ln = Tm, $n = 1$ (**12′**)), and $[Cu_2Ln(L)_2(NO_3)_2(MeOH)(H_2O)]NO_3{\cdot}n$(MeOH) (Ln = Eu, $n = 1$ (**6′**); Ln = Tb, $n = 1$ (**8′**); Ln = Dy, $n = 1$ (**9′′**); Ln = Ho, $n = 1$ (**10′**); Ln = Er, $n = 1$ (**11′**); Ln = Y, $n = 0.5$ (**15′**)). These complexes were heated at 100 °C in vacuo to afford $[Cu_2Ln(L)_2(NO_3)_3]{\cdot}nH_2O$ (Ln = La, $n = 0$ (**1**); Ln = Ce, $n = 0$ (**2**); Ln = Pr, $n = 0$ (**3**); Ln = Nd, $n = 0$ (**4**); Ln = Sm, $n = 0$ (**5**); Ln = Eu, $n = 0$ (**6**); Ln = Gd, $n = 0$ (**7**); Ln = Tb, $n = 1$ (**8**); Ln = Dy, $n = 1$ (**9**); Ln = Ho, $n = 1$ (**10**); Ln = Er, $n = 1$ (**11**); Ln = Tm, $n = 1$ (**12**); Ln = Y, $n = 1$ (**15**)). A portion of **1′**, **4′**, **5′**, **6′**, and **7′** was dissolved in dmf, and the solution was diffused with diethyl ether to form single crystals of the general formula $[Cu_2Ln(L)_2(NO_3)_3(dmf)_2]{\cdot}dmf{\cdot}0.5Et_2O$ (Ln = La (**1′′**), Nd (**4′′**), Sm (**5′′**), Eu (**6′′**), Gd (**7′′**)).

Procedure 2 (13, 14). This is essentially the same as procedure 1 except for the use of triethylamine (2.0 mmol). The volume of the reaction mixture was concentrated to ca. 40 cm^3 and allowed to stand to obtain green crystals (**13′**, **14′**) of the general formula $[Cu_2Ln(L)_2(NO_3)_2(MeOH)(H_2O)]NO_3{\cdot}n$(MeOH) (Ln = Yb, $n = 0$ (**13′**); Ln = Lu, $n = 1$ (**14′**)). These complexes were heated at

(29) Xu, Z.; Read, P. W.; Hibbs, D. E.; Hursthouse, M. B.; Malik, K. M. A.; Patrick, B. O.; Rettig, S. J.; Seid, M.; Summers, D. A.; Pink, M.; Thompson, R. C.; Orvig, C. *Inorg. Chem.* **2000**, *39*, 508.
(30) Bayly, S. R.; Xu, Z.; Patrick, B. O.; Rettig, S. J.; Pink, M.; Thompson, R. C.; Orvig, C. *Inorg. Chem.* **2003**, *42*, 1576.
(31) Shiga, T.; Ohba, M.; Okawa, H. *Inorg. Chem. Commun.* **2003**, *6*, 15.
(32) Ohba, M.; Ohtsubo, N.; Shiga, T.; Sakamoto, M.; Ōkawa, H. *Polyhedron* **2003**, *22*, 1905.
(33) Li, Y.-T.; Jiang, Z.-H.; Liao, D.-Z.; Yan, S.-P.; Ma, S.-L.; Li, X.-Y.; Wang, G.-L. *Polyhedron* **1993**, *12*, 2781.
(34) Li, Y.-T.; Jiang, Z.-H.; Ma, S.-L.; Li, X.-Y.; Liao, D.-Z.; Yan, S.-P.; Wang, G.-L. *Polyhedron* **1994**, *13*, 475.
(35) Li, Y.-T.; Liao, D.-Z.; Jiang, Z.-H.; Wang, G.-L. *Polyhedron* **1995**, *14*, 2209.
(36) Sanz, J. L.; Ruiz, R.; Gleizes, A.; Lloret, F.; Faus, J.; Julve, M.; Borras-Almenar, J. J.; Journaux, Y. *Inorg. Chem.* **1996**, *35*, 7384.
(37) Chen, X.-M.; Wu, Y.-L.; Yang, Y.-Y.; Aubin, S. M. J.; Hendrickson, D. N. *Inorg. Chem.* **1998**, *37*, 6186.
(38) Sanada, T.; Suzuki, T.; Kaizaki, S. *J. Chem. Soc., Dalton Trans.* **1998**, 959.
(39) Stemmler, A. J.; Kampf, J. W.; Kirk, M. L.; Atasi, B. H.; Pecoraro, V. L. *Inorg. Chem.* **1999**, *38*, 2807.
(40) Kido, T.; Nagasato, S.; Sunatsuki, Y.; Matsumoto, N. *Chem. Commun.* **2000**, 2113.
(41) Liu, Q.-D.; Gao, S.; Li, J.-R.; Zhou, Q.-Z.; Yu, K.-B.; Ma, B.-Q.; Zhang, S.-W.; Zhang, X.-X.; Jin, T.-Z. *Inorg. Chem.* **2000**, *39*, 2488.
(42) Madalan, A. M.; Roesky, H. W.; Andruh, M.; Noltemeyer, M.; Stanica, N. *Chem. Commun.* **2002**, 1638.
(43) Tang, J.-K.; Li, Y.-Z.; Wang, Q.-L.; Gao, E.-Q.; Liao, D.-Z.; Jiang, Z.-H.; Yan, S.-P.; Cheng, P.; Wang, L.-F.; Wang, G.-L. *Inorg. Chem.* **2002**, *41*, 2188.
(44) Nishihara, S.; Akutagawa, T.; Hasegawa, T.; Nakamura, T. *J. Am. Chem. Soc.* **2003**, *42*, 2480.
(45) Wang, S.; Pang, Z.; Wagner, M. J. *Inorg. Chem.* **1992**, *31*, 5381
(46) Wang, S.; Pang, Z.; Smith, K. D.; Wagner, M. J. *J. Chem. Soc., Dalton Trans.* **1994**, 955.
(47) Chen, L.; Breeze, S. R.; Rousseau, R. J.; Wang, S.; Thompson, L. K. *Inorg. Chem.* **1995**, *34*, 454.
(48) Wang, S.; Pang, Z.; Smith, K. D. L.; Hua, Y.-s.; Deslippe, C.; Wagner, M. J. *Inorg. Chem.* **1995**, *34*, 908.
(49) Chen, X.-M.; Aubin, S. M. J.; Wu, Y.-L.; Yang, Y.-S.; Mak, T. C. W.; Hendrickson, D. N. *J. Am. Chem. Soc.* **1995**, *117*, 9600.
(50) Kahn, M. L.; Mathonière, C.; Kahn, O. *Inorg. Chem.* **1999**, *38*, 3692.
(51) Decurtins, S.; Gross, M.; Schmalle, H. W.; Ferlay, S. *Inorg. Chem.* **1998**, *37*, 2443.
(52) Liang, Y.; Hong, M.; Su, W.; Cao, R.; Zhang, W. *Inorg. Chem.* **2001**, *40*, 4574.
(53) Gheorghe, R.; Andruh, M.; Muller, A.; Schmidtmann, M. *Inorg. Chem.* **2002**, *41*, 5314.
(54) Rizzi, A. C.; Calvo, R.; Baggio, R.; Garland, M. T.; Peña, O.; Perec, M. *Inorg. Chem.* **2002**, *41*, 5609.
(55) Figuerola, A.; Diaz, C.; Ribas, J.; Tangoulis, V.; Granell, J.; Lloret, F.; Mahía, J.; Maestro, M. *Inorg. Chem.* **2003**, *42*, 641.
(56) He, Z.; He, C.; Gao, E.-Q.; Wang, Z.-M.; Yang, X.-F.; Liao, C.-S.; Yan, C.-H. *Inorg. Chem.* **2003**, *42*, 2206.
(57) Sutter, J.-P.; Kahn, M. L.; Kahn, O. *Adv. Mater.* **1999**, *11*, 863.
(58) Kahn, M. L.; Sutter, J.-P.; Golhen, S.; Guionneau, P.; Ouahab, L.; Kahn, O.; Chasseau, D. *J. Am. Chem. Soc.* **2000**, *122*, 3413.
(59) Sutter, J.-P.; Kahn, M. L.; Mörtl, K. P.; Ballou, R.; Porcher, P. *Polyhedron* **2001**, *20*, 1593.
(60) Kahn, M. L.; Ballou, R.; Porcher, P.; Kahn, O.; Sutter, J.-P. *Chem.—Eur. J.* **2002**, *8*, 525.
(61) Fenton, D. E.; Tate, J. R.; Casellato, U.; Tamburini, S.; Vigato, P. A.; Vidali, M. *Inorg. Chim. Acta* **1984**, *83*, 23.

Table 1. CuLnCu Complexes Prepared in This Study and Their Analytical Data

complex	% C found (calcd)	% H found (calcd)	% N found (calcd)	% Cu found (calcd)	yield (%)	IR data (cm^{-1})		
$[Cu_2La(L)_2(NO_3)_3]$ (**1**)	33.06 (33.13)	2.46 (2.35)	7.51 (7.43)	13.25 (13.48)	94	1607	1594	1385
$[Cu_2Ce(L)_2(NO_3)_3]$ (**2**)	32.93 (33.09)	2.32 (2.35)	7.39 (7.42)	13.52 (13.47)	89	1607	1594	1385
$[Cu_2Pr(L)_2(NO_3)_3]$ (**3**)	32.88 (33.06)	2.34 (2.35)	7.39 (7.42)	13.25 (13.46)	97	1607	1594	1385
$[Cu_2Nd(L)_2(NO_3)_3]$ (**4**)	32.80 (32.95)	2.33 (2.34)	7.39 (7.39)	13.38 (13.41)	97	1608	1594	1385
$[Cu_2Sm(L)_2(NO_3)_3]$ (**5**)	32.88 (32.74)	2.41 (2.32)	7.45 (7.34)	13.27 (13.32)	96	1609	1595	1385
$[Cu_2Eu(L)_2(NO_3)_3]$ (**6**)	32.80 (32.68)	2.24 (2.32)	7.30 (7.33)	12.80 (13.30)	97	1609	1595	1385
$[Cu_2Gd(L)_2(NO_3)_3]$ (**7**)	32.41 (32.50)	2.43 (2.31)	7.27 (7.29)	13.43 (13.32)	97	1609	1595	1385
$[Cu_2Tb(L)_2(NO_3)_3]\cdot H_2O$ (**8**)	32.05 (31.85)	2.48 (2.47)	7.18 (7.14)	13.21 (12.96)	94	1613	1596	1385
$[Cu_2Dy(L)_2(NO_3)_3]\cdot H_2O$ (**9**)	31.69 (31.73)	2.50 (2.46)	7.10 (7.12)	12.88 (12.91)	92	1613	1597	1386
$[Cu_2Ho(L)_2(NO_3)_3]\cdot H_2O$ (**10**)	31.65 (31.41)	2.45 (2.45)	7.15 (7.05)	13.11 (12.59)	93	1611	1596	1385
$[Cu_2Er(L)_2(NO_3)_3]\cdot H_2O$ (**11**)	31.41 (31.58)	2.45 (2.45)	7.05 (7.08)	12.59 (12.85)	88	1611	1597	1385
$[Cu_2Tm(L)_2(NO_3)_3]\cdot H_2O$ (**12**)	31.75 (31.53)	2.41 (2.44)	7.11 (7.07)	12.85 (12.83)	82	1615	1598	1385
$[Cu_2Yb(L)_2(NO_3)_3]$ (**13**)	32.09 (31.98)	2.35 (2.27)	7.15 (7.17)	12.98 (13.10)	68	1615	1598	1385
$[Cu_2Lu(L)_2(NO_3)_3]\cdot H_2O$ (**14**)	31.04 (31.34)	2.57 (2.43)	6.86 (7.03)	12.71 (13.01)	62	1612	1597	1385
$[Cu_2Y(L)_2(NO_3)_3]\cdot H_2O$ (**15**)	34.36 (34.30)	2.68 (2.66)	7.65 (7.69)	13.93 (13.96)	87	1610	1597	1385

100 °C in vacuo to afford $[Cu_2Ln(L)_2(NO_3)_2]NO_3\cdot nH_2O$ (Ln = Yb, $n = 0$ (**13**); Ln = Lu, $n = 1$ (**14**)).

Synthesis of the $Zn_2Ln(L)_2$ Complexes (Ln = Lanthanide Ion Except for Tm, Yb, and Lu). To a solution of $Zn(NO_3)_2\cdot 6H_2O$ (1.0 mmol) and $Ln(NO_3)_3\cdot nH_2O$ (0.5 mmol) in hot methanol (ca. 20 cm^3) was added a hot methanolic solution (ca. 20 cm^3) of H_2L (1.0 mmol) and triethylamine (2.0 mmol). The reaction mixture was stirred for a few minutes and allowed to stand to obtain yellow crystals. These complexes were heated at 100 °C in vacuo to afford $[Zn_2Ln(L)_2(NO_3)_3]\cdot nH_2O$ (Ln = La, $n = 2$ (**16**); Ln = Ce, $n = 2$ (**17**); Ln = Pr, $n = 2$ (**18**); Ln = Nd, $n = 2$ (**19**); Ln = Sm, $n = 2$ (**20**); Ln = Eu, $n = 2$ (**21**); Ln = Gd, $n = 2$ (**22**); Ln = Tb, $n = 3$ (**23**); Ln = Dy, $n = 3$ (**24**); Ln = Ho, $n = 3$ (**25**); Ln = Er, $n = 3$ (**26**) Ln = Y, $n = 3$ (**27**)). A complete list of compounds prepared with their numbering and analytical data is given in Table S1 (see the Supporting Information).

X-ray Structure Determination. Data collection for **1′**, **2′**, **3′**, **4′**, **5′**, **6′**, **9′′**, **12′**, **14′**, and **15′**: All measurements were made on a Rigaku/MSC Mercury CCD diffractometer with graphite-monochromated Mo Kα radiation ($\lambda = 0.71070$ Å). The maximum 2θ value is 55.0°. A total of 1240 oscillation images were collected on five sweep settings. Absorption correction was applied. The data were corrected for Lorentz and polarization effects.

Data collection for **1′′**, **4′′**, **5′′**, **6′′**, **7′**, **7′′**, **8′**, **9′**, **10′**, **11′**, and **13′**: All measurements were made on a Rigaku Raxis-Rapid Imaging plate diffractometer with graphite-monochromated Mo Kα radiation. The maximum 2θ value is 54.7° for **4′′**, **10′**, and **13′** and 55.0° for **1′′**, **5′′**, **6′′**, **7′**, **7′′**, **8′**, **9′**, and **11′**. A total of 44 images for **1′′**, **5′′**, **6′′**, **7′**, **7′′**, **8′**, **9′**, **10′**, **11′**, and **13′**, corresponding to 220.0° oscillation angles, were collected. A total of 44 images for **4′′**, corresponding to 222.0° oscillation angles, were collected. The camera radius was 127.40 nm. A symmetry-related absorption correction using the program ABSCOR was applied.[62] The data were corrected for Lorentz and polarization effects.

All calculations were performed using the teXsan crystallographic software package of Molecular Structure Corp. Hydrogen atoms were included but not refined. Crystallographic data for the structures reported in this paper have been deposited at the Cambridge Crystallographic Data Centre (CCDC) as supplementary publication numbers CCDC-217763−217783.

Magnetic Measurements. Magnetic measurements were carried out on a powder sample with a Quantum Design SQUID MPMS-5XL magnetometer, in the temperature range of 2−300 K and under an applied magnetic field of 500 G. Magnetization was measured at 2 K under an applied field up to 5 T. Diamagnetic corrections were applied using Pascal's constants. Effective magnetic moments were calculated by the equation $\mu_{eff} = 2.828(\chi_M T)^{1/2}$.

Elemental Analyses and Spectroscopic Measurements. Elemental analyses of C, H, and N were performed at the Elemental Analysis Service Center of Kyushu University. Copper analyses were done on a Shimadzu AA-680 atomic absorption/flame emission spectrophotometer. Infrared spectra were measured on KBr disks with a Perkin-Elmer Spectrum BX FT-IR system.

Results and Discussion

Preparation. 2,6-Di(acetoacetyl)pyridine (H_2L) has formed a series of $Cu^{II}Ln^{III}Cu^{II}$ complexes with the general formula $Cu_2Ln(L)_2(NO_3)_3$ (Ln = La−Lu except for Pm) by one-pot reaction of the ligand with $Cu(NO_3)_2\cdot 3H_2O$ and $Ln(NO_3)_3\cdot nH_2O$. By a similar method an analogous $Cu^{II}Y^{III}Cu^{II}$ complex has been prepared. Obviously the 1,3-diketonate site appears to be more specific for the small Cu(II) ion in contrast to the 2,6-diacetylpyridine site, which adapts more specifically for large Ln(III) ions. It must be mentioned that

(62) *Program for Absorption Correction*; Rigaku Corp.: Tokyo, Japan, 1995.

Chart 1. Structure Classification by the Coordination Environments around the Ln^{3+} Ions

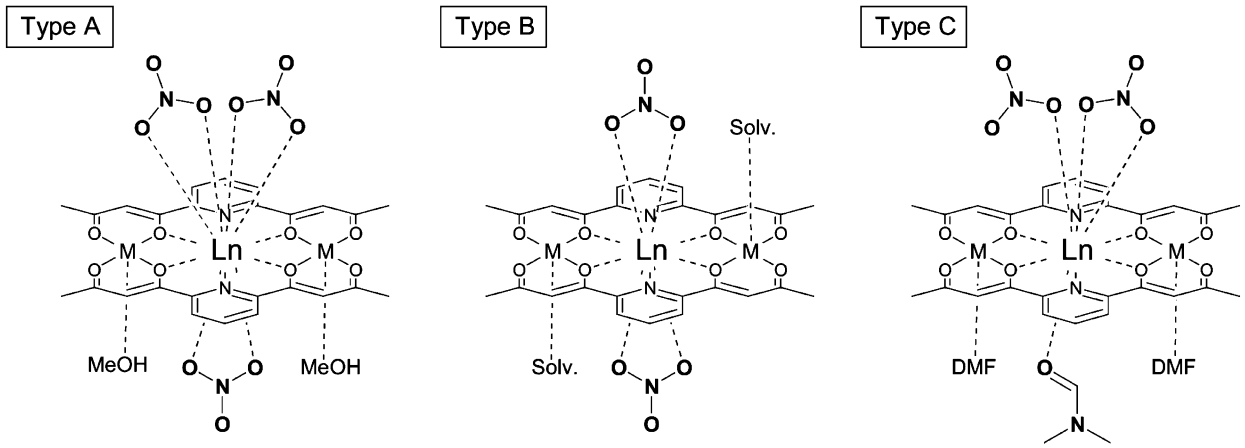

Table 2. Crystal Parameters for Complexes **1′** (A), **14′** (B1), **4′** (B2), **10′** (B3), and **5′** (C)

	1′ (A)	**14′** (B1)	**4′** (B2)	**10′** (B3)	**5″** (C)
empirical formula	$C_{30}H_{38}Cu_2N_5LaO_{21}$	$C_{30}H_{38}Cu_2N_5LuO_{21}$	$C_{30}H_{38}Cu_2N_5NdO_{21}$	$C_{30}H_{38}Cu_2N_5HoO_{21}$	$C_{30}H_{38}Cu_2N_5O_{21}Sm$
fw	1070.65	1056.61	1107.02	1053.63	1082.14
cryst color	green	green	green	green	green
cryst syst	monoclinic	triclinic	triclinic	triclinic	triclinic
space group	*C*2/c (No. 15)	$P\bar{1}$ (No. 2)	$P\bar{1}$ (No. 2)	$P\bar{1}$ (No. 2)	$P\bar{1}$ (No. 2)
a/Å	14.1263(9)	9.640(3)	9.202(3)	7.5524(5)	7.3560(2)
b/Å	17.228(1)	13.689(4)	14.683(4)	9.129(1)	9.6223(3)
c/Å	16.349(1)	13.978(4)	17.225(3)	13.993(1)	15.777(1)
α/deg	90	94.881(4)	66.46(1)	93.095(3)	87.68(1)
β/deg	102.326(3)	102.640(3)	80.74(1)	102.692(3)	88.39(1)
γ/deg	90	101.368(4)	70.18(1)	109.856(4)	63.939(7)
V/Å^3	3887.2500	1748.7081	2006.6044	876.5(1)	1002.2692
Z	4	2	2	1	1
T/°C	−90	−90	−90	−90	−90
λ/Å	0.71070	0.71070	0.71070	0.71070	0.71070
μ(Mo Kα)/ cm^{-1}	22.50	41.00	24.17	35.34	25.88
D_c/g cm^{-3}	1.829	2.007	1.832	1.996	1.793
no. of observations (all)	4356	7714	8783	3909	4467
R^a (all, obsd)	0.051	0.049	0.052	0.066	0.064
$R_w{}^b$ (all, obsd)	0.102	0.101	0.193	0.122	0.136
GOF	1.00	1.00	1.00	1.00	1.00

^{a} $R = \sum||F_o| - |F_c||/\sum|F_o|$. ^{b} $R_w = [\sum[w(|F_o|^2 - |F_c|^2)^2]/\sum w|F_o^2|^2]^{1/2}$.

Cu(II) or Ln(III) alone affords polymeric compounds but not discrete molecular compounds. The complexes of Ln = La−Tm (**1**−**12**) and Ln = Y (**15**) were obtained in a good yield by procedure 1, but the yields for the complexes Cu_2Yb (**13**) and Cu_2Lu (**14**) were extremely low by procedure 1. Eventually, these complexes were prepared in a good yield on adding triethylamine to the reaction mixture (procedure 2).

Description of the Structures. All the complexes have a trinuclear CuLnCu core structure. Two L^{2-} ligands sandwich two Cu(II) ions with the 1,3-diketonate sites and one Ln(III) ion with the 2,6-diacetylpyridine site, forming a nearly planar $\{Cu_2Ln(L)_2\}$ moiety. Two or three nitrate ions are bonded above and below the Ln ion, affording a 10- or 12-coordinate geometry about the metal. The Cu in each complex has a 5-coordinate geometry together with a water or methanol molecule at an axial site. The structures of the complexes are classified into three types (A, B, and C) with respect to the geometry about the central Ln ion (Chart 1). In type A all three nitrate ions are bonded to the Ln ion. Type B has two nitrate ions above and below the Ln ion. Type B is further classified into B1, B2, and B3 with respect to the asymmetric unit structure as discussed below. In type C one DMF molecule is bonded to the Ln ion along with two nitrate ions. The compounds of types A and B were obtained by slow crystallization from methanol, whereas the compounds of type C were obtained by recrystallization from DMF. The crystal parameters for **1′** (A), **14′** (B1), **4′** (B2), **10′** (B3), and **5″** (C) are summarized in Table 2.

Type A. The structure of this type appears only in $[Cu_2La(L)_2(NO_3)_3(MeOH)_2]\cdot MeOH$ (**1′**). ORTEP diagrams of the molecule are shown in Figure 1. Selected bond lengths and angles are given in Table 3. The asymmetric unit consists of half a molecule of $[Cu_2La(L)_2(NO_3)_3(MeOH)_2]$ and half a molecule of MeOH. The two Cu(II) ions are equivalent. The geometry about Cu is square-pyramidal with O(1), O(2), O(3)*, and O(4)* of the two 1,3-diketonate sites on the equatorial plane and O(10) of methanol at the apical position (an asterisk indicates symmetry operation $-x, y, (-z + 1)/2$). The La atom exists in the hexagonal site formed by the two 2,6-diacylpyridine entities and has a 12-coordinate geometry together with O(5), O(6), O(8), O(5)*, O(6)*, and O(8)* of three bidentate nitrate ions. The average equatorial Cu−O, La−O, and La−N bond distances are 1.931, 2.578,

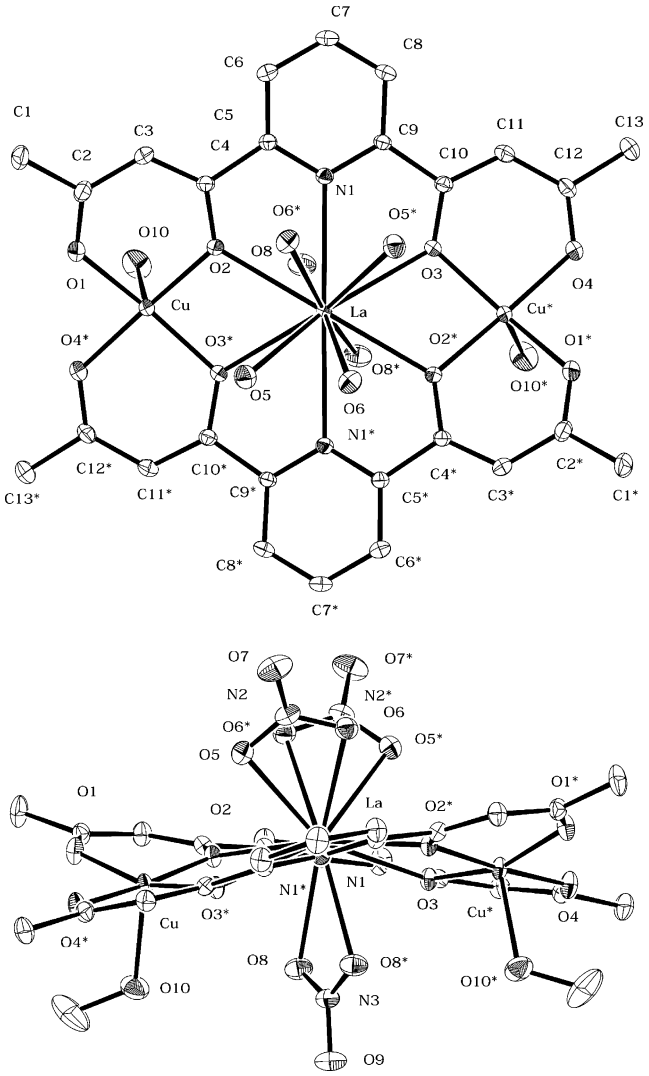

Figure 1. ORTEP drawings of Cu_2La complex **1′** (type A).

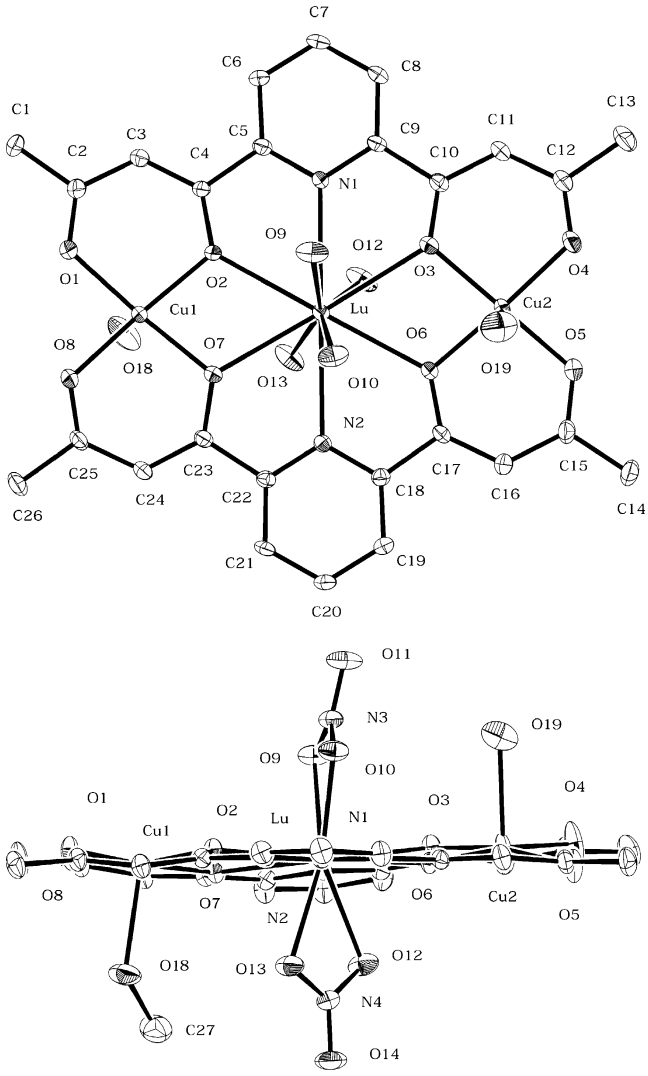

Figure 2. ORTEP drawings of Cu_2Lu complex **14′** (type B1).

Table 3. Selected Bond Lengths and Angles for Complex **1′** (A)[a]

	Bond Lengths (Å)		
La−O(2)	2.533(2)	La−O(3)	2.622(2)
La−O(5)	2.701(2)	La−O(6)	2.708(2)
La−O(8)	2.750(2)	La−N(1)	2.715(2)
Cu−O(1)	1.935(2)	Cu−O(2)	1.923(2)
Cu−O(3)*	1.952(2)	Cu−O(4)*	1.914(2)
Cu−O(10)	2.234(2)		
	Bond Angles (deg)		
O(2)−La−O(3)	115.95(6)	O(2)−La−O(5)	79.65(6)
O(2)−La−O(6)	121.46(6)	O(2)−La−O(8)	65.76(7)
O(2)−La−N(1)	59.38(6)	O(3)−La−O(5)	154.33(6)
O(3)−La−O(6)	109.03(6)	O(3)−La−O(8)	73.04(7)
O(3)−La−N(1)	59.14(6)	O(5)−La−O(6)	46.89(7)
O(5)−La−O(8)	132.49(7)	O(5)−La−N(1)	124.13(7)
O(6)−La−O(8)	167.77(6)	O(6)−La−N(1)	127.83(7)
O(8)−La−N(1)	63.93(6)	O(1)−Cu−O(2)	92.20(9)
O(1)−Cu−O(3)*	160.52(9)	O(1)−Cu−O(4)*	87.41(9)
O(1)−Cu−O(10)	96.01(9)	O(3)*−Cu−O(4)*	93.95(8)
O(3)*−Cu−O(10)	107.06(9)	O(4)*−Cu−O(10)	88.77(9)
La−O(2)−Cu	109.14(8)	La−O(3)−Cu*	104.85(7)

[a] An asterisk indicates symmetry operation $-x, y, (-z + 1)/2$.

and 2.715 Å, respectively. The intermetallic Cu···La and Cu···Cu* separations of the trinuclear core are 3.648(0) and 7.153(1) Å, respectively. One MeOH molecule is free from coordination and resides between the trinuclear molecules. The $\{Cu_2La(L)_2\}$ moiety shows a distortion from coplanarity. The two L^{2-} ligands are twisted at the La atom with a dihedral angle of 23.2° between the two pyridine rings. The shortest Cu···Cu, Cu···La, and La···La intermolecular separations are 7.1521(8), 8.5775(3), and 9.3932(2) Å, respectively.

Type B. The structures of type B are classified into B1 (**6′**, **9″**, **11′**, **12′**, **14′**, **15′**), B2 (**2′**, **3′**, **4′**), and B3 (**5′**, **7′**, **8′**, **9′**, **10′**, **13′**) on the basis of molecular symmetry. The asymmetric unit of type B1 consists of one $[Cu_2Ln(L)_2(NO_3)_2(solv)_2]^+$ cation, one NO_3^- anion, and one MeOH molecule (solv = MeOH or H_2O). The crystal of type B2 has two distinguishable $[Cu_2Ln(L)_2(NO_3)_2(MeOH)_2]^+$ cations, and the asymmetric unit consists of one of the cations, one NO_3^- anion, and three MeOH molecules. The asymmetric unit of type B3 consists of half a molecule of the $[Cu_2Ln(L)_2(NO_3)_2(solv)_2]^+$ cation and half a molecule of the NO_3^- anion (and half a molecule of MeOH for **8′**, **9′**, and **10′**).

As an example of type B1, the structure of $[Cu_2Lu(L)_2(NO_3)_2(MeOH)(H_2O)]NO_3{\cdot}MeOH$ (**14′**) is shown in Figure 2. Selected bond lengths and angles are given in Table 4. The two Cu(II) ions are not equivalent. The Cu(1) atom is

Table 4. Selected Bond Lengths and Angles for Complex **14′** (B1)

Bond Lengths (Å)			
Lu−O(2)	2.482(2)	Lu−O(3)	2.557(2)
Lu−O(6)	2.464(2)	Lu−O(7)	2.494(2)
Lu−O(9)	2.376(3)	Lu−O(10)	2.382(3)
Lu−O(12)	2.371(3)	Lu−O(13)	2.367(3)
Lu−N(1)	2.675(3)	Lu−N(2)	2.626(3)
Cu(1)−O(1)	1.922(3)	Cu(1)−O(2)	1.932(2)
Cu(1)−O(7)	1.929(2)	Cu(1)−O(8)	1.930(2)
Cu(1)−O(16)	2.250(3)	Cu(2)−O(3)	1.922(3)
Cu(2)−O(4)	1.922(3)	Cu(2)−O(5)	1.915(3)
Cu(2)−O(6)	1.933(2)	Cu(2)−O(15)	2.287(4)
Bond Angles (deg)			
O(2)−Lu−O(3)	119.39(8)	O(2)−Lu−O(6)	172.20(7)
O(2)−Lu−O(7)	60.22(7)	O(2)−Lu−O(9)	78.38(9)
O(2)−Lu−O(10)	112.43(9)	O(2)−Lu−O(12)	93.09(10)
O(2)−Lu−O(13)	81.11(10)	O(2)−Lu−N(1)	60.20(8)
O(2)−Lu−N(2)	119.73(8)	O(3)−Lu−O(6)	60.21(8)
O(3)−Lu−O(7)	170.16(9)	O(3)−Lu−O(9)	74.41(9)
O(3)−Lu−O(10)	92.01(9)	O(3)−Lu−O(12)	68.18(9)
O(3)−Lu−O(13)	119.46(9)	O(3)−Lu−N(1)	59.38(8)
O(3)−Lu−N(2)	120.88(8)	O(6)−Lu−O(7)	121.70(8)
O(6)−Lu−O(9)	108.30(9)	O(6)−Lu−O(10)	75.24(9)
O(6)−Lu−O(12)	79.51(10)	O(6)−Lu−O(13)	92.40(10)
O(6)−Lu−N(1)	118.16(8)	O(6)−Lu−N(2)	61.13(8)
O(7)−Lu−O(9)	96.23(9)	O(7)−Lu−O(10)	79.69(9)
O(7)−Lu−O(12)	121.34(9)	O(7)−Lu−O(13)	70.38(9)
O(7)−Lu−N(1)	120.10(8)	O(7)−Lu−N(2)	60.65(8)
O(9)−Lu−O(10)	53.07(9)	O(9)−Lu−O(12)	130.84(8)
O(9)−Lu−O(13)	159.2(1)	O(9)−Lu−N(1)	66.43(9)
O(9)−Lu−N(2)	118.66(8)	O(10)−Lu−O(12)	153.5(1)
O(10)−Lu−O(13)	134.89(9)	O(10)−Lu−N(1)	118.40(9)
O(10)−Lu−N(2)	66.59(9)	O(12)−Lu−O(13)	53.46(9)
O(12)−Lu−N(1)	67.46(9)	O(12)−Lu−N(2)	107.67(9)
O(13)−Lu−N(1)	105.80(9)	O(13)−Lu−N(2)	69.46(9)
N(1)−Lu−N(2)	174.91(7)	O(1)−Cu(1)−O(2)	97.9(1)
O(1)−Cu(1)−O(7)	166.7(1)	O(1)−Cu(1)−O(8)	84.7(1)
O(1)−Cu(1)−O(16)	94.0(1)	O(2)−Cu(1)−O(7)	80.57(10)
O(2)−Cu(1)−O(8)	175.8(1)	O(2)−Cu(1)−O(16)	95.8(1)
O(7)−Cu(1)−O(8)	96.2(1)	O(7)−Cu(1)−O(16)	99.3(1)
O(8)−Cu(1)−O(16)	87.2(1)	O(3)−Cu(2)−O(4)	95.6(1)
O(3)−Cu(2)−O(5)	169.4(1)	O(3)−Cu(2)−O(6)	81.6(1)
O(3)−Cu(2)−O(15)	96.0(1)	O(4)−Cu(2)−O(5)	84.8(1)
O(4)−Cu(2)−O(6)	173.1(1)	O(4)−Cu(2)−O(15)	96.4(2)
O(5)−Cu(2)−O(6)	96.7(1)	O(5)−Cu(2)−O(15)	94.4(1)
O(6)−Cu(2)−O(15)	90.2(1)	Lu−O(2)−Cu(1)	109.89(10)
Lu−O(3)−Cu(2)	107.36(10)	Lu−O(6)−Cu(2)	110.6(1)
Lu−O(7)−Cu(1)	109.40(9)		

in a square-pyramidal geometry with O(1), O(2), O(7), and O(8) of the two 1,3-diketonate sites on the equatorial plane and O(18) of methanol at the apical position. The Cu(2) atom also has a square-pyramidal geometry with O(19) of water at the apical position. The Lu atom exists in the hexagonal site formed by the two 2,6-diacylpyridine entities and has a 10-coordinate geometry together with O(9), O(10), O(12), and O(13) of the two bidentate nitrate ions. The average equatorial Cu−O, Lu−O, and Lu−N bond distances are 1.926, 2.499, and 2.651 Å, respectively. The intermetallic Cu(1)···Lu, Cu(2)···Lu, and Cu(1)···Cu(2) separations are 3.625(1), 3.629(1), and 7.252(2) Å, respectively. One MeOH molecule and one nitrate ion are free from coordination and captured in the lattice. The trinuclear $\{Cu_2Ln(L)_2\}$ moiety is not coplanar; the dihedral angle between the two pyridine rings about Lu is 15.4°. The shortest Cu···Cu, Cu···Lu, and Lu···Lu intermolecular separations are 7.168(1), 6.9621(9), and 7.3057(8) Å, respectively.

Type B2 has a structure essentially the same as that of type B1, but there are two nonequivalent trinuclear cations in the unit cell. The structure of $[Cu_2Nd(L)_2(NO_3)_2(MeOH)_2]$-$NO_3$·3MeOH (**4′**) is discussed as a representative. ORTEP diagrams of the cationic part are shown in Figure 3. Selected bond lengths and angles are given in Table 5. The Cu(1) atom has a square-pyramidal geometry with O(1), O(2), O(3)*, and O(4)* of the two 1,3-diketonate sites on the equatorial plane and O(18) of methanol at the apical position (an asterisk indicates symmetry operation $-x, -y, -z$). The Cu(2) atom also has a square-pyramidal geometry with O(19) of methanol at the apical position. The Nd(1) atom in the hexagonal site formed by the two 2,6-diacylpyridine entities has a 10-coordinate geometry together with O(9), O(10), O(9)*, and O(10)* of the two bidentate nitrate ions. The Nd-(2) atom also has a 10-coordinate geometry together with the two bidentate nitrate ions. The average equatorial Cu−O, Nd−O, and Nd−N bond distances are 1.928, 2.575, and 2.757 Å, respectively. The intermetallic Cu(1)···Nd(1), Cu(2)···Nd(2), Cu(1)···Cu(1)*, and Cu(2)···Cu(2)** separations are 3.650(1), 3.641(1), 7.301(2), and 7.282(2) Å, respectively (two asterisks indicate symmetry operation $-x$, $-y + 1$, $-z$). Three MeOH molecules are captured in the crystal lattice. The trinuclear $\{Cu_2Nd(L)_2\}$ moiety is coplanar with respect to the two L^{2-} ligands; the average dihedral angle between the two pyridine rings about Nd is 0°. The shortest Cu···Cu, Cu···Nd, and Nd···Nd intermolecular separations are 7.3237(6), 7.1771(6), and 7.3417(1) Å, respectively.

Type B3 has the most symmetric structure among the B types. The structure of $[Cu_2Ho(L)_2(NO_3)_2(MeOH)(H_2O)]$-$NO_3$·MeOH (**10′**) is shown in Figure 4 as an example. Selected bond lengths and angles are given in Table 6. Each Cu atom has a square-pyramidal geometry with a methanol or water molecule at the apical position. The Ho atom in the site formed by the two 2,6-diacylpyridine entities has a 10-coordinate geometry together with O(5), O(6), O(5)*, and O(6)* of the two bidentate nitrate ions (an asterisk indicates symmetry operation $-x, -y, -z$). The nitrate ions show a structural disorder due to an inversion along the N(2)−O(7) axis. The average equatorial Cu−O, Ho−O, and Ho−N bond distances are 1.920, 2.504, and 2.672 Å, respectively. The intermetallic Cu···Ho and Cu···Cu* separations are 3.637-(1) and 7.273(1) Å, respectively. One MeOH molecule and one nitrate ion are captured in the crystal lattice. The trinuclear $\{Cu_2Ho(L)_2\}$ moiety is coplanar with respect to the two L^{2-} ligands; the dihedral angle between the two pyridine rings about Ho is 0°. The shortest Cu···Cu, Cu···Ho, and Ho···Ho intermolecular separations are 7.520-(1), 7.2283(8), and 7.5524(5) Å, respectively.

Type C. Complexes of this type (**1″**, **4″**, **5″**, **6″**, and **7″**) were obtained by crystallization from DMF. The structure of $[Cu_2Sm(L)_2(NO_3)_3(dmf)_2]$·dmf·0.5$Et_2O$ (**5″**) is shown in Figure 5 as an example. Selected bond lengths and angles are given in Table 7. The asymmetric unit consists of $[Cu_2$-$Sm(L)_2(NO_3)_3(dmf)_2]$, one dmf molecule, and half a molecule of Et_2O. The two Cu(II) ions are not equivalent. The Cu(1) atom has a square-pyramidal geometry with O(19) of dmf at the apical position. The apical dmf shows a structural disorder due to an inversion along the O(19)−N(7) axis. The

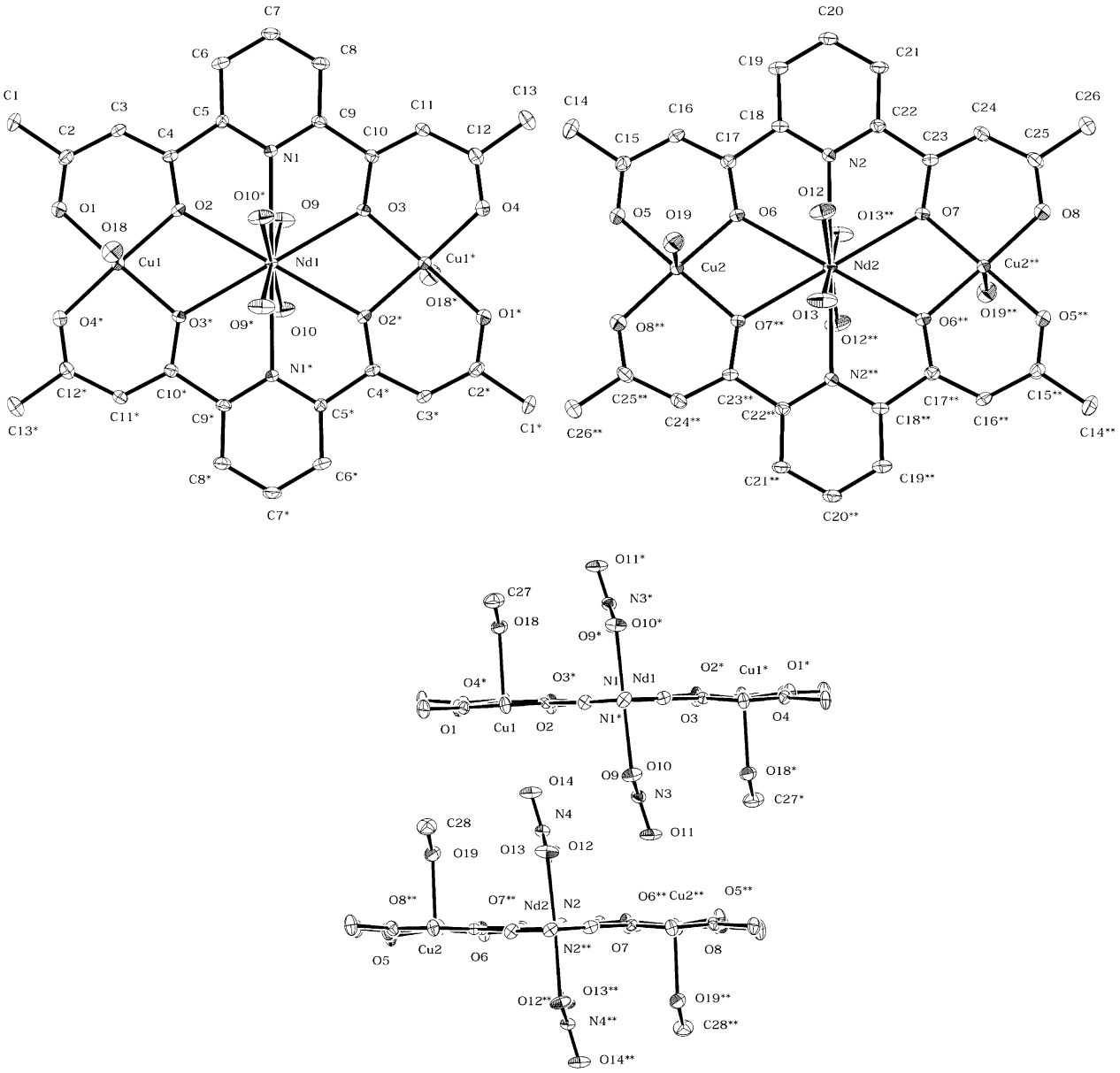

Figure 3. ORTEP drawings of Cu_2Nd complex **4′** (type B2).

Cu(2) atom also has a square-pyramidal geometry with O(15) of the nitrate ion at the apical position. The Sm atom has a 10-coordinate geometry together with O(9) and O(10) of the bidentate nitrate ion, O(12) of the unidentate nitrate ion, and O(18) of dmf. The two nitrate ions are located on the same side with respect to the mean molecular plane. The intermetallic Cu(1)···Sm, Cu(2)···Sm, and Cu(1)···Cu(2) separations are 3.616(1), 3.685(1), and 7.254(1) Å, respectively. Half a molecule of Et_2O and a dmf molecule exist in the crystal lattice. The crystal is extremely efflorescent, and the Et_2O molecule shows a large positional fluctuation. Therefore, the Et_2O molecule was isotropically refined under restricted conditions. The shortest Cu···Cu, Cu···Sm, and Sm···Sm intermolecular separations are 7.410(1), 8.4373(5), and 8.8488(4) Å, respectively.

Structural characteristics of the complexes are summarized in Table 8. It must be emphasized that only a small change occurs in the ionic radius of Ln(III) on going from La(III) to Lu(III). This fact means that the Ln-to-donor distances are regulated by the two $\{CuO_4\}$ chromophores. In accord with this, the Cu−Ln and Cu−Cu interatomic separations show no distinct change with Ln ions. A large dihedral angle is observed for type A (24.90° for **1′**). Type C compounds show a moderate twist between the two pyridine rings (13.46−15.60°). Type B1 has a small dihedral angle of 4.44−5.81°. Type B2 and type B3 show no twist between the two pyridine rings.

Magnetic Properties. Cryomagnetic properties of **1**−**15** were studied in the temperature range of 2−300 K under an applied field of 500 G. The results are discussed in three groups. Group I includes Cu_2La (**1**), Cu_2Lu (**14**), and Cu_2Y (**15**) complexes with a diamagnetic Ln(III) or Y(III) ion. Group II contains only the Cu_2Gd complex (**7**), where Gd(III) has no orbital angular momentum. The remaining

Table 5. Selected Bond Lengths and Angles for Complex **4′** (B2)[a]

Bond Lengths (Å)			
Nd(1)−O(2)	2.560(3)	Nd(1)−O(3)	2.539(3)
Nd(1)−O(9)	2.566(3)	Nd(1)−O(10)	2.509(3)
Nd(1)−N(1)	2.686(3)	Nd(2)−O(6)	2.553(3)
Nd(2)−O(7)	2.537(3)	Nd(2)−O(12)	2.518(3)
Nd(2)−O(13)	2.559(3)	Nd(2)−N(2)	2.692(4)
Cu(1)−O(1)	1.922(3)	Cu(1)−O(2)	1.931(3)
Cu(1)−O(3)*	1.930(3)	Cu(1)−O(4)*	1.913(3)
Cu(1)−O(18)	2.297(4)	Cu(2)−O(5)	1.916(3)
Cu(2)−O(6)	1.933(3)	Cu(2)−O(7)**	1.929(3)
Cu(2)−O(8)**	1.906(3)	Cu(2)−O(19)	2.317(4)
Bond Angles (deg)			
O(2)−Nd(1)−O(3)	119.86(9)	O(2)−Nd(1)−O(9)	78.5(1)
O(2)−Nd(1)−O(10)	103.01(1)	O(2)−Nd(1)−N(1)	59.7(1)
O(3)−Nd(1)−O(9)	73.2(1)	O(3)−Nd(1)−O(10)	97.2(1)
O(3)−Nd(1)−N(1)	60.27(10)	O(9)−Nd(1)−O(10)	49.7(1)
O(9)−Nd(1)−N(1)	64.8(1)	O(10)−Nd(1)−N(1)	114.5(1)
O(6)−Nd(2)−O(7)	119.55(9)	O(6)−Nd(2)−O(12)	78.2(1)
O(6)−Nd(2)−O(13)	102.1(1)	O(6)−Nd(2)−N(2)	59.5(1)
O(7)−Nd(2)−O(12)	81.5(1)	O(7)−Nd(2)−O(13)	106.4(1)
O(7)−Nd(2)−N(2)	60.19(10)	O(12)−Nd(2)−O(13)	49.7(1)
O(12)−Nd(2)−N(2)	65.4(1)	O(13)−Nd(2)−N(2)	115.1(1)
O(1)−Cu(1)−O(2)	95.1(1)	O(1)−Cu(1)−O(3)*	174.9(1)
O(1)−Cu(1)−O(4)*	85.8(1)	O(2)−Cu(1)−O(3)*	82.9(1)
O(2)−Cu(1)−O(4)*	170.3(1)	O(3)*−Cu(1)−O(4)*	95.4(1)
O(5)−Cu(2)−O(6)	95.2(1)	O(5)−Cu(2)−O(7)**	173.9(1)
O(5)−Cu(2)−O(8)**	85.4(1)	O(6)−Cu(2)−O(7)**	83.1(1)
O(6)−Cu(2)−O(8)**	174.1(1)	O(7)*−Cu(2)−O(8)**	95.7(1)

[a] An asterisk indicates symmetry operation $-x, -y, -z$, and two asterisks indicate symmetry operation $-x, -y + 1, -z$.

complexes (**2**−**6** and **8**−**13**) belong to group III. The Ln(III) of this group has an orbital angular momentum. Magnetic analyses for group III have been carried out using analogous Zn_2Ln complexes as the references. In the following analysis of the magnetic data, the magnetic interaction between adjacent trinuclear units is neglected because of significant metal−metal separations (>7.1 Å).

Group I (1, 14, and 15). The cryomagnetic property of **1** is shown in Figure 6 in the form of μ_{eff} vs T and χ_M vs T plots. The effective magnetic moment of **1** is 2.80 μ_B at room temperature, and the moment decreases with decreasing temperature. A similar cryomagnetic property was recognized for **14** and **15** (see Figures S1 and S2, respectively, in the Supporting Information). Magnetic analyses for these complexes can be made on the basis of the Bleaney−Bowers equation.[63] The cryomagnetic property of **1** can be well reproduced using the magnetic parameters of $J = -0.51$ cm^{-1}, $g = 2.14$, and $N\alpha = 420 \times 10^{-6}$ cm^3 mol^{-1} (solid line in Figure 6). The discrepancy factor $R(\chi_M)$ defined in eq 1 was 1.40×10^{-2}, and $R(\mu_{eff})$ defined in eq 2 was 3.99×10^{-3}.

$$R(\chi_M) = [\sum(\chi_{obsd} - \chi_{calcd})^2/\sum(\chi_{obsd})^2]^{1/2} \quad (1)$$

$$R(\mu_{eff}) = [\sum(\mu_{eff,obsd} - \mu_{eff,calcd})^2/\sum(\mu_{eff,obsd})^2]^{1/2} \quad (2)$$

Similarly, the cryomagnetic properties of **14** and **15** are well simulated. The best-fit parameters for **14** are $J = -0.39$ cm^{-1}, $g = 2.13$, and $N\alpha = 500 \times 10^{-6}$ cm^3 mol^{-1} with $R(\chi_M) = 5.77 \times 10^{-3}$ and $R(\mu_{eff}) = 3.26 \times 10^{-3}$, and those for **15** are $J = -0.47$ cm^{-1}, $g = 2.15$, and $N\alpha = 120 \times 10^{-6}$ cm^3 mol^{-1} with $R(\chi_M) = 1.39 \times 10^{-2}$ and $R(\mu_{eff}) = 4.48 \times 10^{-3}$.

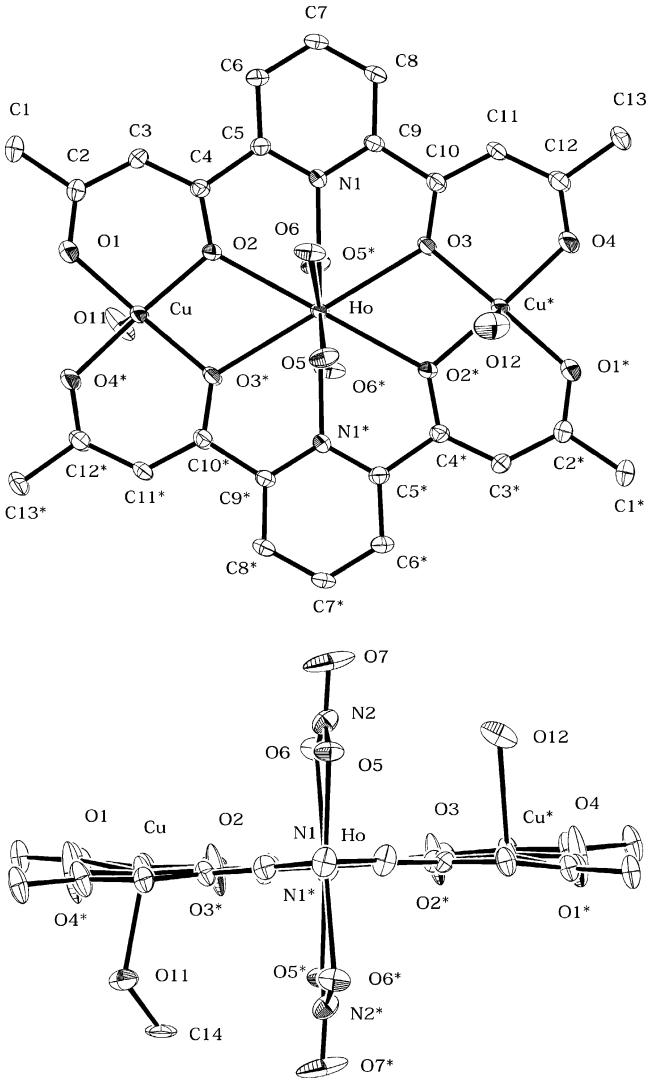

Figure 4. ORTEP drawings of Cu_2Ho complex **10′** (type B3).

The field dependence of magnetization for **1**, **14**, and **15** was measured at 2 K, and the M vs H curve of **1** is shown in Figure 7. The magnetization under 5 T is close to 2 Nβ. In Figure 7 is also given the Brillouin function for two isolated Cu(II) ions ($g = 2.14$). The observed magnetization is smaller than the Brillouin function over the magnetic field range of 0−5 T, adding support to the weak antiferromagnetic interaction between the two terminal copper ions.

Group II (7). The magnetic behavior of **7** is shown in Figure 8. The effective magnetic moment at room temperature is 8.30 μ_B, which is close to the spin-only value (8.31 μ_B) expected for two magnetically isolated Cu(II) ions and one Gd(III) ion. The moment increased with decreasing temperature up to 9.74 μ_B at 3 K. The maximum moment is close to the spin-only value for $S_T = 9/2$ (9.95 μ_B) resulting from the ferromagnetic interaction of the metal ions. The spin Hamiltonian for the $Cu^{II}Gd^{III}Cu^{II}$ system is expressed as follows:

$$\hat{H} = -2J(S_{Cu1}\cdot S_{Gd} + S_{Cu2}\cdot S_{Gd}) \quad (3)$$

(63) Bleaney, B.; Bowers, K. D. *Proc. R. Soc. London, Ser. A* **1952**, *214*, 451.

Table 6. Selected Bond Lengths and Angles for Complex **10′** (B3)[a]

Bond Lengths (Å)			
Ho−O(2)	2.480(3)	Ho−O(3)	2.528(3)
Ho−O(5)	2.513(6)	Ho−O(5′)	2.333(6)
Ho−O(6)	2.533(6)	Ho−O(6′)	2.345(6)
Ho−N(1)	2.672(3)	Cu−O(1)	1.911(3)
Cu−O(2)	1.928(3)	Cu−O(3)*	1.929(3)
Cu−O(4)*	1.911(4)	Cu−O(11)	2.158(6)
Cu−O(12)*	2.476(12)		
Bond Angles (deg)			
O(2)−Ho−O(3)	120.06(9)	O(2)−Ho−O(5)	59.94(9)
O(2)−Ho−O(5′)	88.3(2)	O(2)−Ho−O(6)	76.1(2)
O(2)−Ho−O(6′)	94.1(2)	O(2)−Ho−N(1)	60.33(9)
O(3)−Ho−O(5)	99.1(2)	O(3)−Ho−O(5′)	114.6(2)
O(3)−Ho−O(6)	79.6(2)	O(3)−Ho−O(6′)	64.8(2)
O(3)−Ho−N(1)	59.73(10)	O(5)−Ho−O(6)	50.3(2)
O(5)−Ho−O(6′)	47.8(2)	O(5)−Ho−N(1)	114.8(2)
O(5′)−Ho−O(6)	49.5(2)	O(5′)−Ho−O(6′)	54.7(2)
O(5′)−Ho−N(1)	112.7(2)	O(6)−Ho−N(1)	64.9(1)
O(1)−Cu−O(2)	97.4(1)	O(1)−Cu−O(3)*	168.6(2)
O(1)−Cu−O(4)*	85.0(1)	O(1)−Cu−O(11)	92.1(3)
O(2)−Cu−O(3)*	80.9(1)	O(2)−Cu−O(4)*	174.8(2)
O(2)−Cu−O(11)	102.1(2)	O(3)*−Cu−O(4)*	95.9(1)
O(4)*−Cu−O(11)	82.4(3)	Ho−O(2)−Cu	110.6(1)
Ho−O(3)−Cu*	108.6(1)		

[a] An asterisk indicates symmetry operation $-x, -y, -z$.

where J means the exchange integral between the adjacent Cu(II) and Gd(III) ions. The magnetic susceptibility expression for the $Cu^{II}Gd^{III}Cu^{II}$ system is given as follows:

$$\chi_M = \frac{Ng^2\beta^2}{4k(T-\theta)}\frac{FU}{FD} + N\alpha$$

$$FU = 165\exp(16x) + 84\exp(7x) + 35 + 84\exp(9x) \quad (4)$$

$$FD = 5\exp(16x) + 4\exp(7x) + 3 + 4\exp(9x)$$

with $x = J/kT$. In this expression N is Avogadro's number, β is the Bohr magneton, k is teh Boltzmann constant, J is the exchange integral as defined above, T is the absolute temperature, $N\alpha$ is the temperature-independent paramagnetism, and g is the Lande g factor. θ is included as a correction term for interaction between the terminal Cu(II) ions. The cryomagnetic property of **7** can be simulated by eq 4 using the best-fit parameters $J = +1.41$ cm^{-1}, $g = 1.99$, $\theta = -0.11$ K, and $N\alpha = 120 \times 10^{-6}$ cm^3 mol^{-1}. $R(\chi_M)$ was 3.21×10^{-3}, and $R(\mu_{eff})$ was 3.18×10^{-3}.

The positive J indicates a ferromagnetic interaction between the Cu(II) and Gd(III) ions, and the negative θ means an antiferromagnetic interaction between the terminal Cu(II) ions. The field dependence of the magnetization is shown in Figure 9. The magnetization per Cu_2Gd is 9.05 $N\beta$ at 2 K under 5 T. The Brillouin function for $S = 9/2$ is also shown in Figure 9 (solid line), where $g = 1.99$ is used. The Brillouin function agrees well with the observed magnetization, adding support to teh ferromagnetic interaction between the Cu(II) and Gd(III) ions.

Group III (2−6 and 8−13). The temperature dependencies of the magnetic moments of group III are shown in Figures 10 and 11 together with those of groups I (**1**, **14** and **15**) and II (**7**). The magnetic moments at room temperature are summarized in Table 9. As the starting point of discussion, the room-temperature magnetic moments are

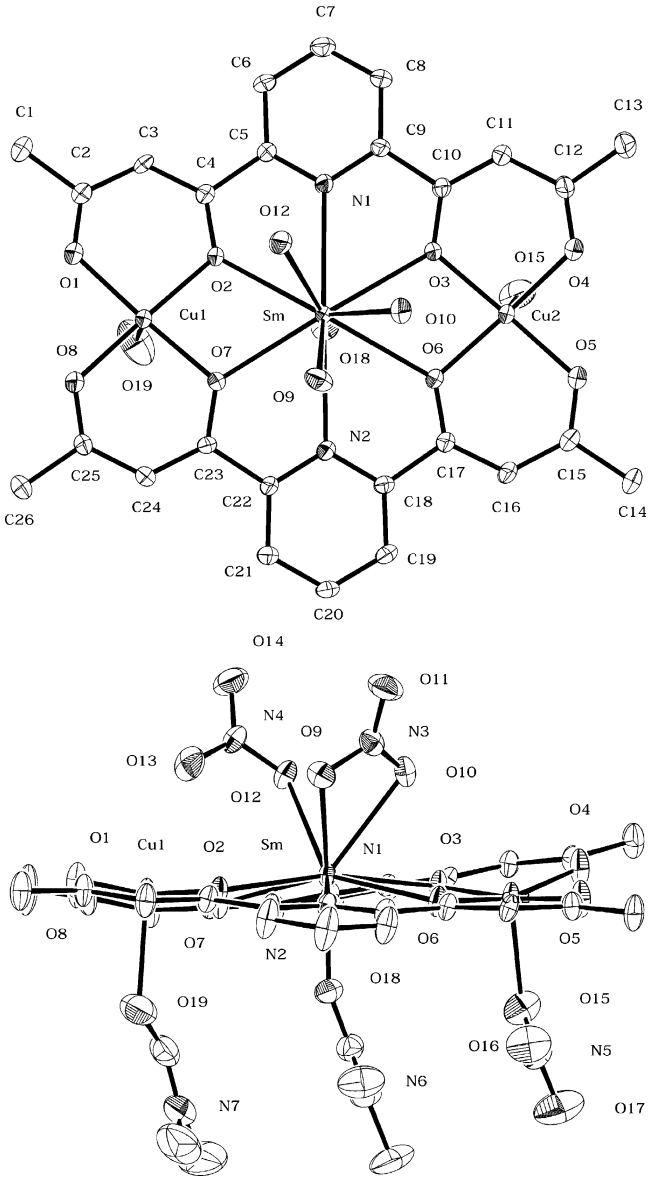

Figure 5. ORTEP drawings of Cu_2Sm complex **5″** (type C).

compared with the expected values for magnetically isolated two Cu(II) ions and one Ln(III) ion. The theoretical magnetic moments μ_{calcd} for the trinuclear complexes are obtained by

$$\mu_{calcd} = [2[4S_{Cu}(S_{Cu}+1)] + g_J{}^2J(J+1)]^{1/2} \quad (5)$$

where g_J is the g factor of the ground J level of each Ln(III) and is expressed as

$$g_J = \frac{3}{2} + \frac{S(S+1) - L(L+1)}{2J(J+1)} \quad (6)$$

The magnetic moments calculated by eq 5 are also given in Table 9. It is seen from Table 9 that the observed magnetic moments are close to the respective expected values for the case of **5** (Ln = Sm) and **6** (Ln = Eu); in these complexes Sm(III) and Eu(III) show a subnormal magnetic moment due to the presence of thermally accessible excited states. Obviously, the magnetic interaction between the Cu(II) and Ln(III) ions is weak in group III.

Table 7. Selected Bond Lengths and Angles for Complex **5′** (C)

Bond Lengths (Å)			
Sm−O(2)	2.547(3)	Sm−O(3)	2.556(3)
Sm−O(6)	2.592(3)	Sm−O(7)	2.523(3)
Sm−O(9)	2.509(3)	Sm−O(10)	2.588(3)
Sm−O(12)	2.505(3)	Sm−O(18)	2.309(3)
Sm−N(1)	2.698(3)	Sm−N(2)	2.740(3)
Cu(1)−O(1)	1.915(3)	Cu(1)−O(2)	1.936(3)
Cu(1)−O(7)	1.931(3)	Cu(1)−O(8)	1.916(3)
Cu(1)−O(19)	2.322(5)	Cu(2)−O(3)	1.933(3)
Cu(2)−O(4)	1.932(3)	Cu(2)−O(5)	1.911(3)
Cu(2)−O(6)	1.931(3)	Cu(2)−O(15)	2.281(4)
Bond Angles (deg)			
O(2)−Sm−O(3)	117.39(9)	O(2)−Sm−O(6)	155.5(1)
O(2)−Sm−O(7)	60.44(9)	O(2)−Sm−O(9)	116.1(1)
O(2)−Sm−O(10)	135.3(1)	O(2)−Sm−O(12)	69.53(10)
O(2)−Sm−O(18)	77.6(1)	O(2)−Sm−N(1)	59.29(9)
O(2)−Sm−N(2)	115.99(9)	O(3)−Sm−O(6)	59.29(9)
O(3)−Sm−O(7)	167.9(1)	O(3)−Sm−O(9)	114.0(1)
O(3)−Sm−O(10)	65.3(1)	O(3)−Sm−O(12)	96.28(10)
O(3)−Sm−O(18)	84.1(1)	O(3)−Sm−N(1)	58.77(9)
O(3)−Sm−N(2)	117.41(9)	O(6)−Sm−O(7)	117.03(9)
O(6)−Sm−O(9)	84.5(1)	O(6)−Sm−O(10)	67.75(10)
O(6)−Sm−O(12)	133.5(1)	O(6)−Sm−O(18)	77.9(1)
O(6)−Sm−N(1)	116.01(9)	O(6)−Sm−N(2)	58.46(9)
O(7)−Sm−O(9)	75.81(10)	O(7)−Sm−O(10)	125.45(10)
O(7)−Sm−O(12)	93.89(9)	O(7)−Sm−O(18)	83.8(1)
O(7)−Sm−N(1)	119.92(9)	O(7)−Sm−N(2)	58.88(9)
O(9)−Sm−O(10)	49.8(1)	O(9)−Sm−O(12)	69.6(1)
O(9)−Sm−O(18)	142.2(1)	O(9)−Sm−N(1)	135.3(1)
O(9)−Sm−N(2)	65.6(1)	O(10)−Sm−O(12)	66.0(1)
O(10)−Sm−O(18)	142.2(1)	O(10)−Sm−N(1)	99.28(10)
O(10)−Sm−N(2)	96.54(10)	O(12)−Sm−O(18)	143.2(1)
O(12)−Sm−N(1)	67.80(10)	O(12)−Sm−N(2)	131.76(10)
O(18)−Sm−N(1)	81.6(1)	O(18)−Sm−N(2)	77.6(1)
N(1)−Sm−N(2)	159.17(10)	O(1)−Cu(1)−O(2)	95.8(1)
O(1)−Cu(1)−O(7)	173.4(2)	O(1)−Cu(1)−O(8)	85.9(1)
O(1)−Cu(1)−O(19)	95.4(2)	O(2)−Cu(1)−O(7)	82.6(1)
O(2)−Cu(1)−O(8)	176.8(1)	O(2)−Cu(1)−O(19)	90.9(1)
O(7)−Cu(1)−O(8)	95.4(1)	O(7)−Cu(1)−O(19)	91.0(2)
O(8)−Cu(1)−O(19)	91.7(2)	O(3)−Cu(2)−O(4)	94.6(1)
O(3)−Cu(2)−O(5)	172.8(2)	O(3)−Cu(2)−O(6)	82.4(1)
O(3)−Cu(2)−O(15)	90.8(1)	O(4)−Cu(2)−O(5)	84.9(1)
O(4)−Cu(2)−O(6)	163.3(2)	O(4)−Cu(2)−O(15)	93.4(2)
O(5)−Cu(2)−O(6)	96.0(1)	O(5)−Cu(2)−O(15)	96.5(2)
O(6)−Cu(2)−O(15)	103.0(2)	Sm−O(2)−Cu(1)	106.8(1)
Sm−O(3)−Cu(2)	109.6(1)	Sm−O(6)−Cu(2)	108.2(1)
Sm−O(7)−Cu(1)	107.9(1)		

The magnetic interaction of group III can be inspected from the temperature variation of the magnetic moment given in Figures 10 and 11 and from the field dependence of the magnetization given in Figures 12 and 13. The operation of ferromagnetic interaction is suggested for **8** (Cu_2Tb) and **9** (Cu_2Dy) judged from the increase in magnetic moment at low temperature. The complexes of group III are classified into two on the basis of the field dependence of the magnetization. The M vs H curves of **2**−**6** show a slow increase with applied field to reach a small magnetization (1.5−2.6 Nβ) at 5 T (Figure 12). The operation of antiferromagnetic interaction in **2**−**4** is most likely because the magnetization of **4** (Cu_2Nd) and **5** (Cu_2Sm) each is small relative to that of group I (**1**, **14**, and **15**) over the applied field of 0−5 T. On the other hand, complexes **8**−**11** show a sharp increase in magnetization with applied field to reach a large value (6.6−7.3 Nβ) at 5 T (Figure 13). The operation of ferromagnetic interaction in **8** (Cu_2Tb) and **9** (Cu_2Dy) is mentioned above on the basis of the temperature variation of the magnetic moment. We suppose that complexes **10** (Cu_2Ho) and **11** (Cu_2Er) also show ferromagnetic interaction between the Cu(II) and Ln(III) ions.

To elucidate the nature of the magnetic interaction between the Cu(II) and Ln(III) ions, an empirical approach based on

Table 8. Summary of Structural Characteristics of the Complexes

		intermetallic separation (Å)		dihedral	bond distance (Å)		
complex	type	Cu−Ln	Cu−Cu	angle (deg)	Cu−O	Ln−O	Ln−N
Cu_2La (**1′**)	A	3.648	7.153	24.90	1.931	2.578	2.715
Cu_2La (**1″**)	C	3.689	7.279	13.87	1.930	2.602	2.774
Cu_2Ce (**2′**)	B2	3.651	7.301	0	1.932	2.560	2.713
Cu_2Pr (**3′**)	B2	3.645	7.290	0	1.926	2.548	2.696
Cu_2Nd (**4′**)	B2	3.646	7.292	0	1.923	2.547	2.689
Cu_2Nd (**4″**)	C	3.673	7.273	13.46	1.928	2.575	2.757
Cu_2Sm (**5′**)	B3	3.642	7.283	0	1.924	2.531	2.695
Cu_2Sm (**5″**)	C	3.651	7.254	14.79	1.926	2.555	2.719
Cu_2Eu (**6′**)	B1	3.648	7.295	4.42	1.925	2.526	2.675
Cu_2Eu (**6″**)	C	3.654	7.261	15.60	1.926	2.552	2.713
Cu_2Gd (**7′**)	B3	3.649	7.298	0	1.924	2.491	2.674
Cu_2Gd (**7″**)	C	3.644	7.249	15.58	1.927	2.543	2.701
Cu_2Tb (**8′**)	B3	3.648	7.295	0	1.925	2.516	2.666
Cu_2Dy (**9′**)	B3	3.650	7.300	0	1.920	2.520	2.668
Cu_2Dy (**9″**)	B1	3.636	7.272	5.20	1.922	2.515	2.662
Cu_2Ho (**10′**)	B3	3.637	7.273	0	1.920	2.504	2.672
Cu_2Er (**11′**)	B1	3.624	7.246	5.81	1.922	2.505	2.653
Cu_2Tm (**12′**)	B1	3.638	7.276	4.44	1.923	2.506	2.655
Cu_2Yb (**13′**)	B3	3.633	7.267	0	1.915	2.506	2.658
Cu_2Lu (**14′**)	B1	3.627	7.252	6.07	1.926	2.499	2.651
Cu_2Y (**15′**)	B1	3.641	7.282	4.51	1.924	2.508	2.665

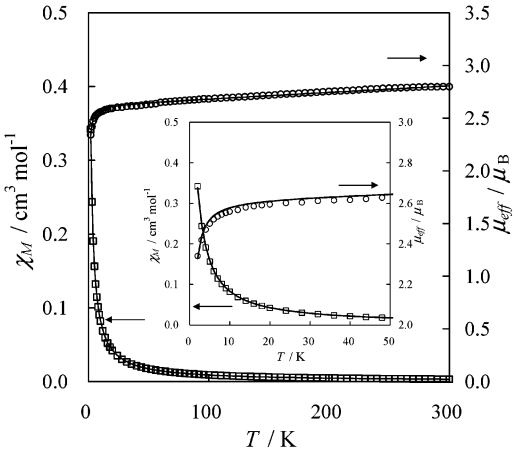

Figure 6. χ_M vs T and μ_{eff} vs T plots of **1**. The solid lines represent the theoretical curves (see the text).

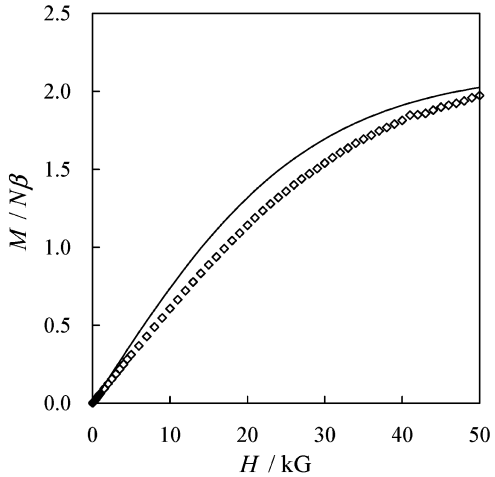

Figure 7. M vs H curve for **1**. The solid line indicates the theoretical curve for $S = 1/2 + 1/2$ ($g = 2.14$).

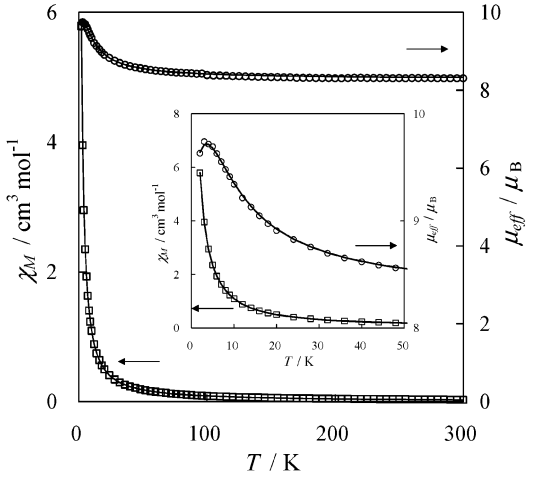

Figure 8. χ_M vs T and μ_{eff} vs T plots of **7**. The solid lines represent the theoretical curves (see the text).

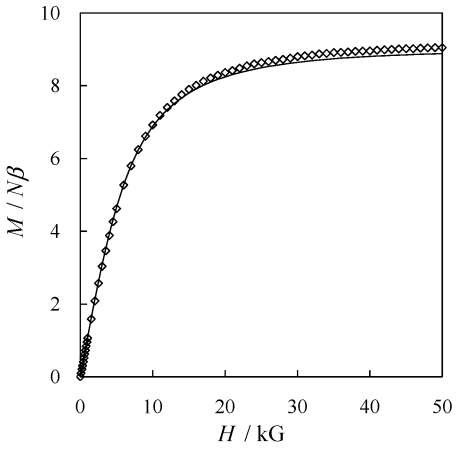

Figure 9. M vs H curve for **7**. The solid line indicates the theoretical curve for $S = 9/2$ ($g = 1.99$).

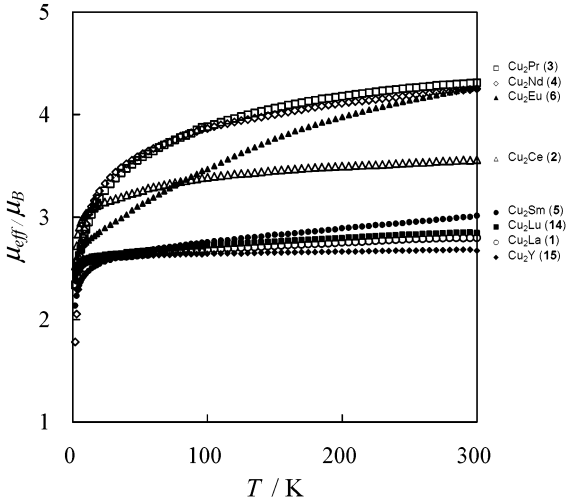

Figure 10. μ_{eff} vs T plots for complexes **1**−**6**, **14**, and **15**: ○, **1**; △, **2**; □, **3**; ◇, **4**; ●, **5**; ▲, **6**; ■, **14**; ◆, **15**.

comparison with analogous Zn_2Ln complexes is adopted. The differences in the $\chi_M T$ values between Cu_2Ln and Zn_2Ln complexes, $\Delta(\chi_M T) = (\chi_M T)_{Cu_2Ln} - (\chi_M T)_{Zn_2Ln}$, are shown in Figures 14 and 15. At room temperature, the $\Delta(\chi_M T)$ values for **2**−**5** fall in the range of 0.78−0.90 $cm^3\ mol^{-1}$ K, which are close to 0.75 $cm^3 mol^{-1} K$ expected for two isolated

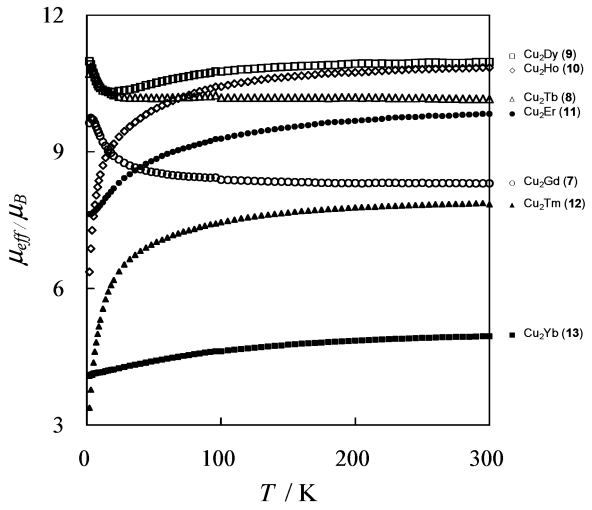

Figure 11. μ_{eff} vs T plots for complexes **7**−**13**: ○, **7**; △, **8**; □, **9**; ◇, **10**; ●, **11**; ▲, **12**; ■, **13**.

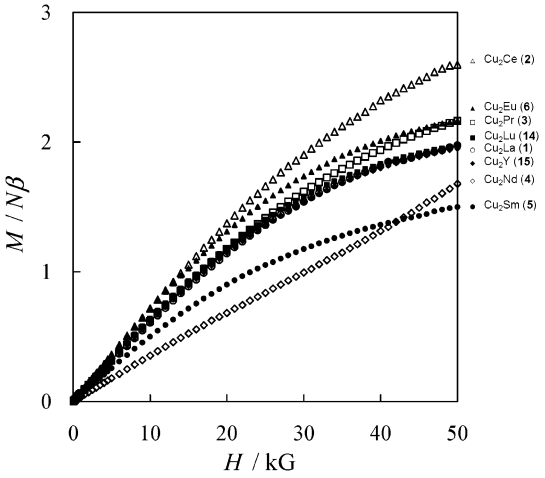

Figure 12. M vs H plots for complexes **1**−**6**, **14**, and **15**: ○, **1**; △, **2**; □, **3**; ◇, **4**; ●, **5**; ▲, **6**; ■, **14**; ◆, **15**.

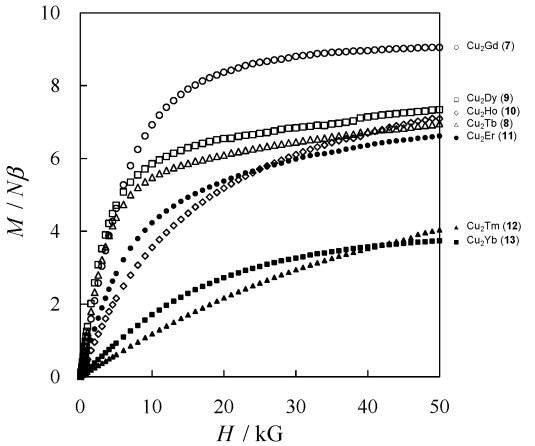

Figure 13. M vs H plots for complexes **7**−**13**: ○, **7**; △, **8**; □, **9**; ◇, **10**; ●, **11**; ▲, **12**; ■, **13**.

Cu(II) ions, assuming a g value. In the case of **2**−**5**, $\Delta(\chi_M T)$ decreased with decreasing temperature (Figure 14). This fact is taken as an indication of antiferromagnetic interaction between the Cu(II) and Ln(III) ions. In the case of **6** (Ln = Eu(III)), the $\Delta(\chi_M T)$ value is almost independent of temperature (Figure 14). This magnetic behavior may be explained

Table 9. $\mu_{eff,calcd}$ Values for Complexes **1**−**15** Calculated from Eq 5 and Observed Effective Magnetic Moments, $\mu_{eff,obsd}$, at 300 K

complex		no. of f electrons	$\mu_{eff,calcd}$	$\mu_{eff,obsd}$
Cu_2La	(**1**)	0	2.45	2.80
Cu_2Ce	(**2**)	1	3.53	3.56
Cu_2Pr	(**3**)	2	4.34	4.31
Cu_2Nd	(**4**)	3	4.37	4.25
Cu_2Sm	(**5**)	5	2.59	3.01
Cu_2Eu	(**6**)	6	2.45	4.26
Cu_2Gd	(**7**)	7	8.31	8.30
Cu_2Tb	(**8**)	8	10.02	10.16
Cu_2Dy	(**9**)	9	10.92	10.97
Cu_2Ho	(**10**)	10	10.89	10.85
Cu_2Er	(**11**)	11	9.89	9.83
Cu_2Tm	(**12**)	12	7.95	7.85
Cu_2Yb	(**13**)	13	5.15	4.95
Cu_2Lu	(**14**)	14	2.45	2.81
Cu_2Y	(**15**)	0	2.45	2.67

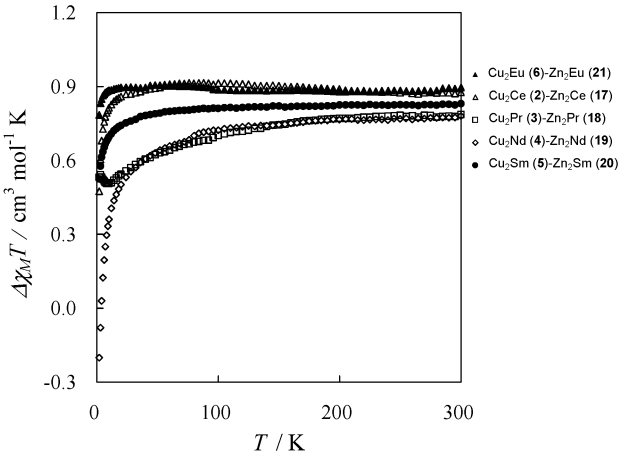

Figure 14. $\Delta\chi_M T$ vs T plots for complexes **2**−**6**: △, **2**; □, **3**; ◇, **4**; ●, **5**; ▲, **6**.

by the fact that Eu(III) is nonmagnetic at low temperature due to its $^4F_0$ ground term. At very low temperature ($T < 4$ K), the $\Delta(\chi_M T)$ value slightly decreased probably due to weak antiferromagnetic interaction between two Cu(II) ions. In the case of **7**−**11**, the $\Delta(\chi_M T)$ values are generally larger than 0.75 $cm^3\ mol^{-1}$ K for two isolated Cu(II) ions and increase with decreasing temperature, indicating ferromagnetic interaction between the adjacent Cu(II) and Ln(III) ions (Figure 15). In the case of **3** (Cu_2Pr) and **10** (Cu_2Ho), the magnetic behavior below 13 K could not be interpreted well. However, the essential magnetic interaction can be explained as antiferromagnetic for **3** and ferromagnetic for **10**. Such an empirical approach for elucidating magnetic interaction could not be adopted for **12** (Ln = Tm), **13** (Yb), and **14** (Lu) because their analogous Zn_2Ln complexes have not been obtained.

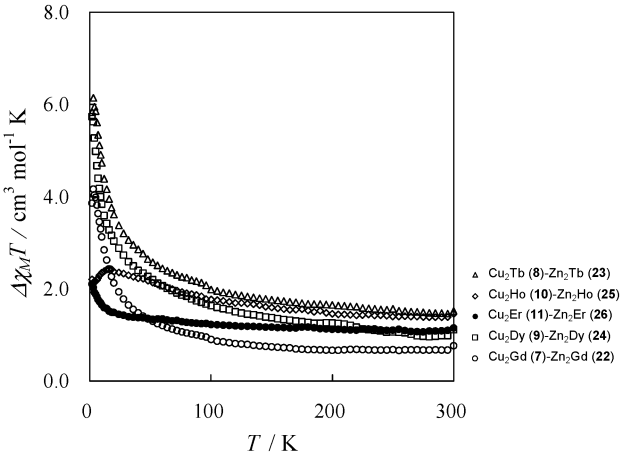

Figure 15. $\Delta\chi_M T$ vs T plots for complexes **7**−**11**: ○, **7**; △, **8**; □, **9**; ◇, **10**; ●, **11**.

Conclusion

A series of trinuclear CuLnCu complexes of general formula $Cu_2Ln(L)_2(NO_3)_3$ have been prepared with 2,6-di-(acetoacetyl)pyridine (H_2L) as the bridging ligand, by employing a one-pot reaction with $Cu(NO_3)_2 \cdot 3H_2O$ and $Ln(NO_3)_3 \cdot nH_2O$. Single-crystal structures of all the lanthanide series except Pm have been determined. Cryomagnetic studies for the complexes with diamagnetic La(III), Lu(III), or Y(III) (**1**, **14**, and **15**) demonstrated a weak antiferromagnetic interaction between the two terminal Cu(II) ions. In the case of **7** with a Gd(III) ion, a ferromagnetic interaction occurs between the Cu(II) and Gd(III) ions. Numerical magnetic studies for other complexes indicate the presence of an antiferromagnetic interaction for **2** (Cu_2Ce), **3** (Cu_2Pr), **4** (Cu_2Nd), and **5** (Cu_2Sm) and a ferromagnetic interaction for **8** (Cu_2Tb), **9** (Cu_2Dy), **10** (Cu_2Ho), and **11** (Cu_2Er).

Acknowledgment. This work was supported by the Grant-in-Aid for Scientific Research Program (No. 13640561) from the Ministry of Education, Culture, Sports, Science and Technology and Precursory Research for Embryonic Science and Technology (PRESTO), JST, Japan.

Supporting Information Available: Table of analytical data of Zn_2Ln complexes and crystal parameters for Cu_2Ln complexes, and the μ_{eff} vs T plots for complexes **14** (Figure S1) and **15** (Figure S2) with a theoretical curve (see the text) (PDF). This material is available free of charge via the Internet at http://pubs.acs.org.

IC034998L